Renormalization-group analysis of chiral transitions

Hikaru Kawamura*
Institute for Physical Science and Technology, University of Maryland, College Park, Maryland 20742
(Received 29 February 1988)

Chiral phase transitions are analyzed by renormalization-group techniques on the basis of a standard Ginzburg-Landau-Wilson Hamiltonian for two real n-component fields $\mathbf{a}$ and $\mathbf{b}$ with quartic couplings $u(\mathbf{a}^2+\mathbf{b}^2)^2$ and $v[(\mathbf{a}\cdot\mathbf{b})^2-\mathbf{a}^2\mathbf{b}^2]$. This model is a natural extension of the usual φ^4 O(n) model: For $v>0$, it represents triangular antiferromagnets, helical magnets, and the A phase of superfluid ^{3}He. An $\epsilon=4-d$ expansion reveals a new $v>0$, *chiral fixed point* which is stable for $n>21.8-23.4\epsilon+O(\epsilon^2)$. An antisymmetric *chirality tensor*, $\kappa=a_\lambda b_\mu-a_\mu b_\lambda$, is a new relevant operator at this fixed point. The associated exponents γ and ν are smaller than the usual O(n) exponents. A $1/n$ expansion yields a continuous chiral transition for $2<d<4$, the exponents γ and ν again being smaller than in the O(n) case. The chiral crossover exponent, ϕ_κ, exceeds γ in both ϵ and $1/n$ expansions. The spectrum of other leading scaling operators and their exponents is obtained. On the basis of comparisons with recent Monte Carlo and experimental results, it is argued that the chiral fixed point probably remains stable down to the physically relevant cases $n=2$ and 3 at $d=3$.

I. INTRODUCTION

Universal features at a critical point are determined by only a few basic parameters characterizing the system under study. In three-dimensional ferromagnets with short-ranged interactions, for example, the number of symmetrically related spin components, n, determines the critical properties; the values $n=1$, 2, 3 correspond to Ising (easy-magnetization-axis anisotropy), XY (easy-magnetization-plane anisotropy), and Heisenberg (isotropic) universality classes, respectively. Renormalization-group theory[1-3] has revealed that the critical behavior of these n-vector systems is governed by an O(n), or isotropic Heisenberg fixed point.

Systematic renormalization-group calculations, including the ε expansion[2,3] and the $1/n$ expansion,[4,5] usually start with an effective Hamiltonian or so-called Ginzburg-Landau-Wilson (GLW) Hamiltonian, which is written in terms of spin variables of unconstrained length rather than of fixed length. For n-vector ferromagnets, this is the standard O(n) or φ^4 model defined by

$$H=\tfrac{1}{2}[(\nabla\boldsymbol{\varphi})^2+r_0\boldsymbol{\varphi}^2+u\boldsymbol{\varphi}^4]\ , \tag{1.1}$$

where $\boldsymbol{\varphi}=(\varphi_1,\varphi_2,\ldots,\varphi_n)$ is a real n-component vector field, while r_0 is a temperature-like variable and $u>0$.

In real magnetic materials, various perturbations, including long-range dipolar interactions, or anisotropic crystalline fields, may change the critical behavior from that of the pure O(n) universality class.[6] Experimentally, however, such effects are usually minor, not only because these perturbations are small in magnitude, causing only a weak crossover from O(n) behavior, but also because the new exponents happen to be rather close numerically to the standard O(n) values. In certain materials, on the other hand, entirely new types of critical behavior may arise. Indeed, on the basis of a symmetry argument and Monte Carlo simulations it has been claimed[7-9] that certain magnetic systems exhibiting *noncollinear spin ordering* should belong to such new universality classes. Examples are helical magnets such as Ho, Dy, Tb, β-MnO_2, and layered triangular XY or Heisenberg antiferromagnets such as VCl_2, VBr_2, and $CsMnBr_3$. In helical magnets, the spins align ferromagnetically in a plane and form a spiral along the orthogonal axis as illustrated in Fig. 1(a). In triangular antiferromagnets, the lattice consists of plane antiferromagnetic triangular lattices stacked in register along the orthogonal axis; the spin ordering is a "120° structure" in which spins on three sublattices align in a plane forming 120° angles with neighboring spins on the other sublattices [see Fig. 1(b)]. It transpires that such systems can be described by the extended GLW Hamiltonian,[7,10,11]

$$H=\tfrac{1}{2}\{\nabla\mathbf{a})^2+(\nabla\mathbf{b})^2+r_0(\mathbf{a}^2+\mathbf{b}^2) +u(\mathbf{a}^2+\mathbf{b}^2)^2+v[(\mathbf{a}\cdot\mathbf{b})^2-\mathbf{a}^2\mathbf{b}^2]\}\ , \tag{1.2}$$

where $\mathbf{a}=(a_1,a_2,\ldots,a_n)$ and $\mathbf{b}=(b_1,b_2,\ldots,b_n)$ are real n-component vector fields, n being the underlying spin dimensionality. The condition $n\geq 2$ is necessary to allow for the appropriate noncollinear orderings. In physical examples, one has $n=2$ (XY spins) or $n=3$ (Heisenberg spins). In helical or triangular antiferromagnets, the $\mathbf{a}$ and $\mathbf{b}$ fields represent the cosine and sine modes associated with the helical spin ordering at wave vectors, $\pm\mathbf{Q}$, via

$$\mathbf{S}(\mathbf{r})=\mathbf{a}(\mathbf{r})\cos(\mathbf{Q}\cdot\mathbf{r})+\mathbf{b}(\mathbf{r})\sin(\mathbf{Q}\cdot\mathbf{r})\ . \tag{1.3}$$

Note that, in this case, the critical fluctuations arise at *two* equivalent but distinct wave vectors $\mathbf{Q}$ and $-\mathbf{Q}$. The existence of two such "instability points" is the origin of the two independent critical fields, $\mathbf{a}$ and $\mathbf{b}$. This should be contrasted with magnetic systems on bipartite lattices,

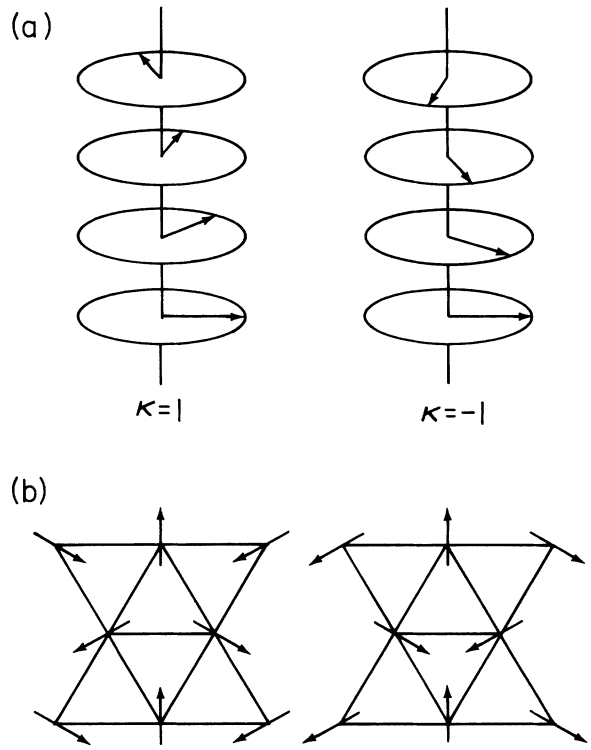

FIG. 1. Illustration of the two energetically degenerate spin structures of opposite chirality, κ, in the ordered states of (a) helical magnets, and of (b) layered triangular antiferromagnets.

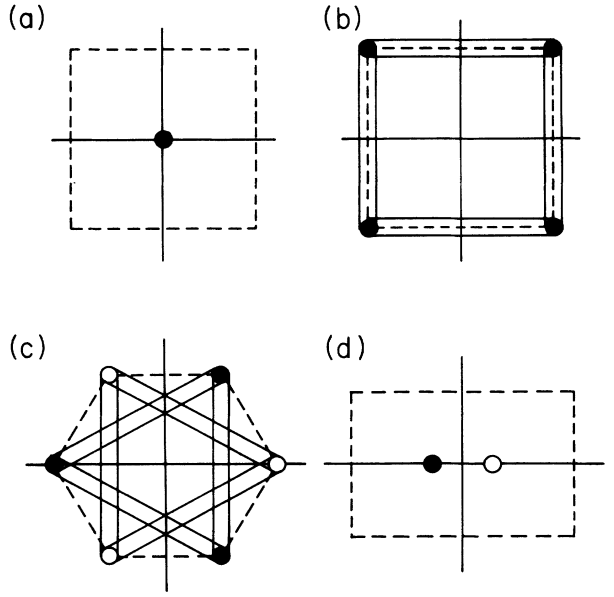

FIG. 2. Representations of "instability points," solid and open circles, in wave-vector space for (a) ferromagnets, (b) antiferromagnets on bipartite lattices, (c) layered triangular antiferromagnets, and (d) helical magnets. The dashed lines outline the first Brillouin zone. Double lines represent the reciprocal-lattice vectors **K**: as usual, points connected by a **K** should be fully identified.

which have only one instability point (see Fig. 2). The dipole-locked A phase of helium 3 can be described by essentially the same GLW Hamiltonian.[12,13]

The purpose of this paper is to investigate the critical properties of the GLW Hamiltonian (1.2) within the framework of renormalization-group ε and $1/n$ expansions, and, in particular, to identify and characterize in detail a new *chiral fixed point* which describes intrinsically noncollinear spin criticality. Chirality is, in fact, inherent in the noncollinear spin orderings. For concreteness, consider a layered triangular XY ($n=2$) antiferromagnet.[9] A local chirality variable κ_p, may be defined on each plaquette, or elementary triangle on the triangular lattice, by

$$\kappa_p=\frac{2}{3\sqrt{3}}\sum_{\langle ij\rangle}^{p}\sin(S_i^xS_j^y-S_i^yS_j^x)\ , \tag{1.4}$$

where the summation runs over the three directed bonds surrounding each plaquette, p. Physically, the chirality represents the sense of the 120° structure or the helix (see Fig. 1). In terms of the GLW Hamiltonian (1.2), this chirality variable, κ, can be generalized to the $n\times n$ antisymmetric tensor,

$$\kappa_{\lambda\mu}=a_\lambda b_\mu-a_\mu b_\lambda\quad(1\le\lambda,\mu\le n)\ . \tag{1.5}$$

For the XY case this reduces simply to $\kappa=a_xb_y-a_yb_x$, which essentially represents (1.4). In the renormalization-group analysis, we find that chirality appears as a new relevant operator at the chiral fixed points. The associated crossover exponent, ϕ_κ, is calculated by both ε and $1/n$ expansions. Unexpectedly, ϕ_κ exceeds the susceptibility exponent γ; however, this turns out to be consistent with a recent Monte Carlo result.[9] The exponents γ and ν are found to be smaller than the corresponding O(n) exponents. More generally, in the space of bilinear spin operators, we find *four* different crossover exponents, including the chiral crossover exponents; by contrast the usual O(n) model, (1.1), has only one bilinear crossover exponent.

The remainder of the paper is arranged as follows. In Sec. II we derive the GLW Hamiltonian (1.2) from various microscopic spin Hamiltonians and analyze its symmetry properties carefully. Section III is devoted to the ε expansion: some of the results have been reported previously,[10–13] but various new results are also presented. A variety of fixed points are identified and their stability is studied to $O(\varepsilon^2)$. In particular, we highlight the chiral fixed point relevant to helical spin ordering. The associated exponents γ and η are calculated to $O(\varepsilon)$ and $O(\varepsilon^2)$, respectively. The $1/n$ expansion is considered in Sec. IV. After summarizing the behavior in the limit $n\to\infty$, the exponents γ, η, and α are calculated to $O(1/n)$. The nature of chiral ordering is studied in Sec. V. The chiral crossover exponent is calculated both by ε and $1/n$ expansions. The crossover exponents for all operators quadratic in the spin variables are calculated in Sec. VI. The corresponding scaling fields are identified and their physical meaning is clarified. Finally, in Sec. VII, we summarize the results and compare them with available Monte Carlo results and experimental data.

II. EFFECTIVE HAMILTONIAN

In this section we discuss several microscopic models which may be described by the GLW Hamiltonian (1.2). As a first example consider an antiferromagnetic Heisenberg model on the stacked-triangular lattice and generalize the model to n-component spins on a d-dimensional lattice in which ($d=2$) triangular lattice layers are stacked in register along the remaining $d-2$ directions in hypercubic fashion. The simplest Hamiltonian is

$$\mathcal{H}=-J\sum_{\langle ij\rangle}\mathbf{S}_i\cdot\mathbf{S}_j-J'\sum_{\langle ij\rangle}\mathbf{S}_i\cdot\mathbf{S}_j,\quad J<0\ , \tag{2.1}$$

where $\mathbf{S}_i$ is an ($n\geq 2$)-component vector of fixed length $|\mathbf{S}_i|=1$. The first sum represents antiferromagnetic interactions in the triangular layers which gives rise to frustration and causes the noncollinear spin ordering; the second sum encompasses the interlayer interaction. The sign of the interlayer interaction, J', is unimportant because there is no frustration along the orthogonal directions. (In fact, J' is antiferromagnetic, in most real materials.) By using the Hubbard-Stratonovich transformation, the fixed-length spins can be replaced by soft spins of unconstrained length. Then, by expanding around the instability points, making a long-wavelength approximation, and dropping terms beyond quartic order, one is led to an effective Hamiltonian (1.2). Some of the details are sketched in Appendix A. As noted previously, the existence of two equivalent, but distinct, instability points, characterized by the wave vectors $\pm\mathbf{Q}$, leads to the two independent fields $\mathbf{a}$ and $\mathbf{b}$, which represent the physical $\cos(\mathbf{Q}\cdot\mathbf{r})$ and $\sin(\mathbf{Q}\cdot\mathbf{r})$ modes, respectively.

The helical Heisenberg model constitutes a second example. In real helical magnets, the origin of the ordering may be the oscillatory nature of the Ruderman-Kittel-Kasuya-Yosida (RKKY) interaction (e.g., Ho, Dy, Tb) or a competition between first- and second-neighbor antiferromagnetic interactions in a body-centered-tetragonal lattice (e.g., β-MnO_2). However, the standard model, frequently used in theoretical analyses, is defined, for $n\geq 2$, by

$$\mathcal{H}=-J_1\sum_{\langle ij\rangle}\mathbf{S}_i\cdot\mathbf{S}_j-J_2\sum_{\langle ij\rangle}\mathbf{S}_i\cdot\mathbf{S}_j \qquad (J_1>0,\ J_2<0)\ , \tag{2.2}$$

where the first term represents ferromagnetic nearest-neighbor interactions, while the second represents antiferromagnetic next-nearest-neighbor interactions which are assumed to act along only one lattice axis, say $(1, 0, 0, \ldots, 0)$. When the ratio J_2/J_1 exceeds a critical value, the system will exhibit helical spin ordering along the $(1, 0, 0, \ldots, 0)$ direction. This helical Heisenberg model also yields the effective Hamiltonian (1.2) (see Appendix A). The only difference from the stacked-triangular antiferromagnets is that the associated $\mathbf{Q}$ vector is now generally incommensurate with the lattice, whereas in the former case, the 120° structure is commensurate. This difference, however, does not affect the effective Hamiltonian up to quartic order.

A final, nonmagnetic example is the dipole-locked A phase of helium 3, which corresponds to $n=3$. Since the associated GLW Hamiltonian is discussed by Moore and co-workers,[12,13] we shall not present details here. Note, however, that the complex vector field $\boldsymbol{\phi}$ in Refs. 12 and 13 corresponds to $(\mathbf{a}+i\mathbf{b})/\sqrt{2}$ in (1.2), while the two quartic couplings g and λ are given by $g=2(4u-v)$ and $\lambda=2v$.

As mentioned, one can specify (1.2) purely by symmetry considerations: the Hamiltonian is invariant under the two independent operations (i) on $O(n)$ rotation in spin space, namely,

$$\mathbf{a}'=R\,\mathbf{a},\ \mathbf{b}'=R\,\mathbf{b},\ R\in O(n)\ , \tag{2.3}$$

and (ii) an O(2) change of phase which mixes the $\mathbf{a}$ and $\mathbf{b}$ fields according to

$$\begin{aligned}\mathbf{a}'&=\cos\theta\,\mathbf{a}-\sin\theta\,\mathbf{b}\ ,\\ \mathbf{b}'&=\pm(\sin\theta\,\mathbf{a}+\cos\theta\,\mathbf{b})\ .\end{aligned} \tag{2.4}$$

This second invariance derives from the arbitrariness in choosing the phase θ and the handedness of the two basic physical modes, $\cos(\mathbf{Q}\cdot\mathbf{r}+\theta)$ and $\pm\sin(\mathbf{Q}\cdot\mathbf{r}+\theta)$. Conversely, if one requires the $O(n)$ rotational invariance as well as the O(2) phase invariance, the form of the effective Hamiltonian is uniquely determined up to fourth order. Note that the individual terms $\mathbf{a}^2\mathbf{b}^2$ and $(\mathbf{a}\cdot\mathbf{b})^2$ are not invariant under (2.4) separately, although the combination

$$(\mathbf{a}\cdot\mathbf{b})^2-\mathbf{a}^2\mathbf{b}^2=-\sum_{\lambda,\mu}^{n}(a_\lambda b_\mu-a_\mu b_\lambda)^2$$

is.

The sign of the quartic coupling v may be regarded as invariant under renormalization to quartic order in $\mathbf{a}$ and $\mathbf{b}$, because the $v=0$ manifold corresponds to the $2n$-component isotropic Heisenberg model which constitutes a separatrix of the standard renormalization-group flows. The relative orientation of the $\mathbf{a}$ and $\mathbf{b}$ fields is dictated by the v term, because all other terms depend only on magnitudes of $\mathbf{a}$ and $\mathbf{b}$. For $v>0$ the fields $\mathbf{a}$ and $\mathbf{b}$ tend to be orthogonal; the resulting spin configuration is

$$\mathbf{s}(\mathbf{r})\simeq\mathbf{a}\cos(\mathbf{Q}\cdot\mathbf{r})+\mathbf{b}\sin(\mathbf{Q}\cdot\mathbf{r})$$

with $\mathbf{a}\perp\mathbf{b}$, which represents *helical* spin ordering. On the other hand, for $v<0$ the fields $\mathbf{a}$ and $\mathbf{b}$ tend to align parallel or antiparallel; this represents a *sinusoidal,* or the linearly-polarized spin-density wave. All the physical examples discussed earlier are associated with noncollinear ordering and, hence, $v>0$. For the magnetic models mentioned, one can also check the positivity of v directly from the derivation of (1.2) in Appendix A. Although our main interest here concerns helical systems, we shall occasionally refer to the sinusoidal case with $v<0$. Lastly, note that the boundedness of the free energy requires

$$u>0 \text{ and } v<4u\ . \tag{2.5}$$

It is instructive at this stage to summarize the results of the mean-field approximation for (1.2). When v is *positive,* a continuous transition takes place at $r_0=0$ between the paramagnetic state and a helical state characterized by

$$|\mathbf{a}|^2=|\mathbf{b}|^2=-r_0/(4u-v)\quad (v>0)\ . \tag{2.6}$$

When v *vanishes* or is *negative,* there is a continuous transition at $r_0=0$ between paramagnetic and sinusoidal states characterized by

$$|\mathbf{a}|^2+|\mathbf{b}|^2=-r_0/2u \quad (v\leq 0) . \tag{2.7}$$

Note that the relative magnitude of **a** and **b** is not now determined; this corresponds physically to the sliding degree of freedom of the spin-density wave. In the mean-field approximation, phase transitions between the paramagnetic and the ordered states are always continuous with classical exponents for any v. Of course fluctuations change these conclusions as we will see.

Finally, note that, in the XY case ($n=2$), one can transform the GLW Hamiltonian (1.2) into the form,[14]

$$\mathcal{H}=\tfrac{1}{2}[(\nabla\mathbf{A})^2+(\nabla\mathbf{B})^2+r_0(\mathbf{A}^2+\mathbf{B}^2) +(u-\tfrac{1}{4}v)(\mathbf{A}^4+\mathbf{B}^4)+2(u+\tfrac{1}{4}v)\mathbf{A}^2\mathbf{B}^2] , \tag{2.8}$$

via the change of variables,

$$\sqrt{2}A_x=a_x+b_y,\quad \sqrt{2}B_x=a_y+b_x ,$$
$$\sqrt{2}A_y=a_y-b_x,\quad \sqrt{2}B_y=-a_x+b_y . \tag{2.9}$$

It follows from this that (1.2) decouples into two independent XY models when $n=2$ and $v=-4u$. However, this special manifold belongs to the sinusoidal region; furthermore, the transformation has no direct counterpart for $n\neq 2$.

III. THE ε EXPANSION

The upper critical dimension for the Hamiltonian (1.2) is $d_>=4$ and a standard renormalization-group $\varepsilon=4-d$ expansion is readily computed. Here the results are summarized; some have appeared previously[10–13] but a few new ones are also reported.

The recursion relations for the quartic couplings were obtained to $O(\varepsilon^2)$ by Jones, Love, and Moore;[12] for completeness we quote them here in our notation:

$$\frac{du}{dl}=\varepsilon u-K[4(n+4)u^2-2(n-1)uv+\tfrac{1}{2}(n-1)v^2] -\tfrac{1}{2}K^2[5(n-1)v^3-39(n-1)uv^2 +88(n-1)u^2v-48(3n+7)u^3] , \tag{3.1}$$

$$\frac{dv}{dl}=\varepsilon v-K[(n-6)v^2+24uv] -\tfrac{1}{2}K^2[(9n-29)v^3-8(n-31)uv^2 -16(5n+41)u^2v] , \tag{3.2}$$

where $K=2^{-d+1}/[\pi^{d/2}\Gamma(d/2)]$. At lowest order in ε, there are up to four fixed points depending on the value of n. Two exist for all n: one is the trivial Gaussian fixed point $G(u^*=v^*=0)$; the other corresponds to the standard isotropic O($2n$) Heisenberg fixed point, H, with $v^*=0$, which is stable provided

$$n<2-\varepsilon+O(\varepsilon^2) . \tag{3.3}$$

To describe the remaining fixed points we consider four distinct regimes of relating n and d:

$$\text{I.}\quad n>n_{\rm I}(d)=12+4\sqrt{6}-[(36+14\sqrt{6})/3]\varepsilon+O(\varepsilon^2) \simeq 21.8-23.4\varepsilon+O(\varepsilon^2) .$$

When n is sufficiently large to meet this condition, two new fixed points appear for $v>0$. They may be termed *chiral,* C_+, and *antichiral,* C_-, the former being stable in accord with the renormalization-group flows sketched in Fig. 3(a). With the notation

$$B_n^{-1}=n^3+4n^2-24n+144$$
and
$$R_n=n^2-24n+48 , \tag{3.4}$$

the fixed point coordinates are given to $O(\varepsilon)$ by

$$Ku_\pm^*=\tfrac{1}{8}B_n[3n^2-2n+24\pm(n-6)R_n^{1/2}]\varepsilon+O(\varepsilon^2) , \tag{3.5}$$

$$Kv_\pm^*=B_n[(n+4)(n-3)\mp 3R_n^{1/2}]\varepsilon+O(\varepsilon^2) . \tag{3.6}$$

The thermal renormalization-group eigenvalue follows for these, and all other fixed points, from the general expression

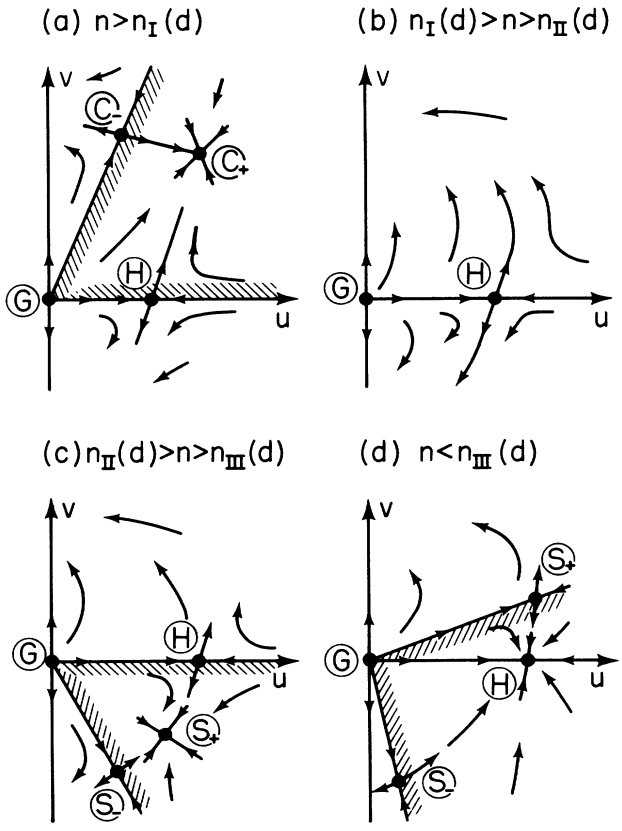

FIG. 3. Renormalization group flows in the (u,v) plane for small $\varepsilon=4-d$. Parts (a)–(d) correspond to the regimes I–IV specified in the text where the borderlines $n_{\rm I}(d)$, $n_{\rm II}(d)$, and $n_{\rm III}(d)$ are given to $O(\varepsilon)$. The hatched regions represent basins of attraction of the most stable fixed point.

$$\lambda_1 = 2 - 4(n+1)Ku^* + (n-1)Kv^* + O(\varepsilon^2) . \quad (3.7)$$

Two further eigenvalues and their eigenvectors follow by linearizing (3.1) and (3.2) around the fixed points in the usual way. For completeness we quote:

$$\lambda_{2\pm} = -\varepsilon + O(\varepsilon^2) ,$$
$$\lambda_{3\pm} = B_n[3R_n \mp (n+4)(n-3)R_n^{1/2}]\varepsilon + O(\varepsilon^2) . \quad (3.8)$$

When n approaches $n_I(d)$ the chiral and antichiral fixed points coalesce at a point in the upper half (u,v) plane and become complex valued.

As usual the exponents γ and ν for the susceptibility and correlation length follow, to $O(\varepsilon)$, from $\gamma \approx 2\nu = 2/\lambda_1$. At the chiral fixed point, C_+, one obtains from (3.5)–(3.7),

$$\gamma \approx 2\nu = 1 + \tfrac{1}{4}B_n[n(n^2+n+48) + (n+4)(n-3)R_n^{1/2}]\varepsilon + O(\varepsilon^2) ,$$
$$\approx 1 + \tfrac{1}{2}(1-9n^{-1})\varepsilon \quad (n \gg 1) . \quad (3.9)$$

Thus these exponents are numerically smaller than those for normal $O(n)$ Heisenberg fixed points for which the coefficient of ε behaves as $\frac{1}{2}(1-6n^{-1})$ for $n \gg 1$.

The critical point decay exponent requires a separate calculation which is outlined in Appendix B. The result to leading order is

$$\eta = \tfrac{1}{8}B_n^2[C_n + (n+4)(n-3)R_n^{3/2}]\varepsilon^2 + O(\varepsilon^3) , \quad (3.10)$$

which varies as $3\varepsilon^2/(4n)$ as $n \to \infty$ since

$$C_n = 5n^5 - 3n^4 - 16n^3 - 656n^2 + 3072n - 1152 . \quad (3.11)$$

Regarding $v < 0$, the sinusoidal case, no stable fixed points are found [see Fig. 3(a)]. This suggests that the transition from paramagnetic to sinusoidal ordering becomes of first order. That conclusion is, indeed, consistent with the exact results recently found[15] for the $n \to \infty$ (or spherical model) limit of the Hamiltonian (1.2) where a first-order transition appears for $3 \le d \le 4$:

II. $n_I(d) > n > n_{II}(d) = 12 - 4\sqrt{6} - [(36 - 14\sqrt{6})/3]\varepsilon + O(\varepsilon^2) \simeq 2.20 - 0.57\varepsilon + O(\varepsilon^2)$.

The renormalization group flows are now as depicted in Fig. 3(b). Only the Gaussian and Heisenberg fixed points are present and both are unstable (for $v \neq 0$). Consequently the transition to both helical and sinusoidal phases is expected to be of first order:

III. $n_{II}(d) > n > n_{III}(d) = 2 - \varepsilon + O(\varepsilon^2)$.

In this regime a new pair of fixed points appear which may be called *sinusoidal*, S_+, and *antisinusoidal*, S_-. Analytically, S_+, which is stable, corresponds to the *antichiral* fixed point, C_-, and the same formulas (3.5)–(3.8) apply; likewise, S_-, which is unstable, corresponds to C_+. The corresponding flows resemble those sketched in Fig. 3(c). The exponent γ can be computed as before (and differs analytically only by the change of sign of the factors containing $R_n^{1/2}$); in this case it turns out to be numerically larger than the corresponding O(n) exponents. In the helical region, $v > 0$, the transition presumably remains of first order since no stable fixed points appear.

As $n \to 2 - \varepsilon + O(\varepsilon^2)$ the sinusoidal fixed point, S_+, approaches the $v = 0$ axis and, at $n = n_{III}(d)$ it meets the Heisenberg fixed point and exchanges stability with it:

IV. $n < n_{III}(d)$.

As illustrated in Fig. 3(d) the fixed point S_+ now lies above the $v = 0$ axis and is unstable; the O($2n$) Heisenberg fixed point H is stable and governs the critical behavior of regions of both helical and sinusoidal ordered behavior.

For the helical region, $v > 0$, which is of primary concern here, the facts concerning the stable fixed points are summarized in Fig. 4. A crucial question is what happens at the physically significant points, $\varepsilon = 1$ with $n = 2$ and 3. Unfortunately, these are rather far from both the $\varepsilon \to 0$ and the $n \to \infty$ limits. Clearly, truly definitive answers cannot be obtained from the present, leading order ε expansion results. Nevertheless, if one linearly extrapolates the small-ε expressions for the stability boundaries to $\varepsilon = 1$, the physical points are found to be included in the stability domain of the chiral fixed point (see Fig. 4). This observation, although certainly not conclusive in itself, seems consistent with recent Monte Carlo results for the $d = 3$ stacked-triangular-lattice antiferromagnets, where a continuous transition has been found both in the XY ($n = 2$) and in the Heisenberg ($n = 3$) cases.[8,9] Thus, it is plausible that the stable chiral fixed point exceeds down to $n = 2$ and 3 at $\varepsilon = 1$. As far as the chiral fixed point remains stable, the critical exponents γ and ν are probably smaller than the corresponding O(n) exponents. A more detailed comparison between the

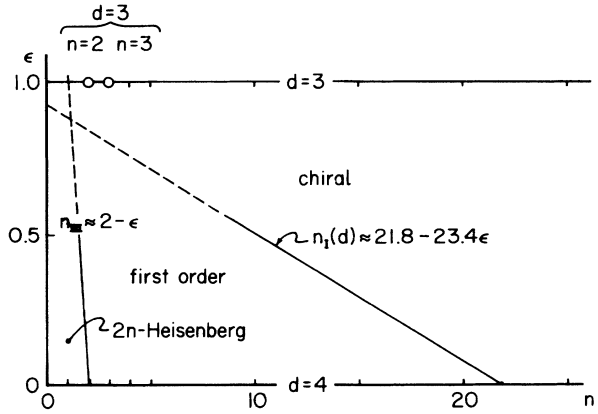

FIG. 4. Stability regions in the (n,d) plane, with $d = 4 - \varepsilon$, of fixed points accessible in the helical region $v > 0$.

renormalization-group results and the Monte Carlo results is presented below in Sec. VII.

Finally, consider the behavior *at* and *above* $d=4$ dimensions. For $d>4$, the transition is governed by the Gaussian fixed point, which is stable, as usual, for all v. At $d=4$ the stability becomes marginal for $v\geq 0$. On the other hand, for $v<0$ and $n>6$ the Gaussian fixed point becomes marginally *unstable* (although remaining marginally stable for $n\leq 6$). Thus a sinusoidally ordering system in $d=4$ dimensions is expected to show a first-order transition when $n>6$.

IV. EXPANSION ABOUT THE $n\rightarrow\infty$ LIMIT

In the many-component limit $n\rightarrow\infty$, the Hamiltonian (1.2) can be solved exactly for arbitrary dimensionality d. A continuous transition with the standard spherical-model exponents, $\alpha=(d-4)/(d-2)$, $\beta=\frac{1}{2}$, and $\gamma=2\nu=2/(d-2)$ arises for $2<d<4$ when $v\geq 0$.[15] An expansion of the exponents from the spherical-model limit in powers of $1/n$ should thus be feasible. On the other hand, for $v<0$ the $n\rightarrow\infty$ behavior is more complex:[15] A single first-order transition appears when $3\leq d\leq 4$, whereas for $2<d<3$, two separate continuous transitions occur; the intermediate phase has no long-range spin order, i.e., $\langle\mathbf{a}\rangle=\langle\mathbf{b}\rangle=0$, but possesses long-range phase coherence, so that $\langle\mathbf{a}\cdot\mathbf{b}\rangle\neq 0$. In view of these complications, this section will focus only on the helical case, $v>0$. [Of course, for $v=0$, the Hamiltonian (1.2) reduces directly to the standard O($2n$) model.]

The calculation proceeds in standard fashion,[5] making the assumption that u and v are both of order $1/n$. [This is consistent with the fixed-point values given in (3.5) and (3.6).] The results found for $2<d<4$ are

$$\alpha=\frac{d-4}{d-2}\left[1+12\frac{d-1}{d-4}\frac{S_d}{n}\right]+O(1/n^2)\ , \tag{4.1}$$

$$\gamma=\frac{2}{d-2}\left[1-9\frac{S_d}{n}\right]+O(1/n^2)\ , \tag{4.2}$$

$$\eta=6[(4/d)-1]S_d/n+O(1/n^2)\ , \tag{4.3}$$

where S_d is given by

$$S_d=\sin[\tfrac{1}{2}\pi(d-2)]\Gamma(d-1)/\{2\pi[\Gamma(\tfrac{1}{2}d)]^2\}\ . \tag{4.4}$$

All other exponents follow through the standard scaling and hyperscaling relations such as $(2-\eta)\nu=\gamma$, $\alpha+2\beta+\gamma=2$, $d\nu=2-\alpha$, etc. The corresponding results for the O(n) model are, of course, well known.[4,5] On comparison, one sees that γ and ν for the present model are *smaller* than the corresponding exponents for O(n) magnets, in agreement with the ε expansion results. One can also check that the $\varepsilon\rightarrow 0$ ($d\rightarrow 4$) limit in (4.1)–(4.4) reproduces the large n behavior of the ε-expansion results (3.9) and (3.10), etc.

In the balance of this section, the calculations are sketched with emphasis on the differences from the standard model. The quartic part of the Hamiltonian (1.2) may be written

$$\mathcal{H}_I=\tfrac{1}{2}\sum_{\lambda,\mu}^{n}[ua_\lambda^2a_\mu^2+ub_\lambda^2b_\mu^2+va_\lambda a_\mu b_\lambda b_\mu +w(a_\lambda^2b_\mu^2+a_\mu^2b_\lambda^2)]\ , \tag{4.5}$$

where $\lambda,\mu=1,2,\ldots,n$ are spin component indices, while

$$w=u-\tfrac{1}{2}v\ . \tag{4.6}$$

The spin-spin correlation functions

$$G_{aa}(\mathbf{k})\equiv\langle a_\lambda(\mathbf{k})a_\lambda(-\mathbf{k})\rangle=G_{bb}(\mathbf{k}) \equiv\langle b_\mu(\mathbf{k})b_\mu(-\mathbf{k})\rangle\ , \tag{4.7}$$

are independent of the indices λ and μ and are equal by symmetry. Likewise, $\langle a_\lambda(\mathbf{k})b_\mu(-\mathbf{k})\rangle$ vanishes identically for all λ and μ. In terms of the true inverse susceptibility

$$r=\chi^{-1}=G^{-1}(0)\ , \tag{4.8}$$

the correlation function can be written

$$G_{aa}^{-1}(\mathbf{k},r)=r+k^2+\Sigma_{aa}(\mathbf{k},r)-\Sigma_{aa}(\mathbf{k}=\mathbf{0},r)\ , \tag{4.9}$$

where $\Sigma_{aa}=\Sigma_{bb}=\Sigma$ is the self-energy, while the propagator is

$$g_{aa}(\mathbf{k})=g_{bb}(\mathbf{k})=(r+k^2)^{-1}\equiv g(\mathbf{k})\ . \tag{4.10}$$

Note that by (4.5) the two external legs attached to any self-energy diagram must both correspond to **a** or both to **b**.

A. Evaluation of η

In order to calculate η, we put $r=0$ ($T=T_c$) and study the small-$\mathbf{k}$ behavior of $G(\mathbf{k},r)\equiv G_{aa}=G_{bb}$, which should be described by

$$G^{-1}(\mathbf{k})\propto k^{2-\eta}\approx k^2(1-\eta\ln k+\cdots)\ . \tag{4.11}$$

The leading self-energy diagrams are shown in Fig. 5 where the wavy lines represent the dressed interactions, with propagators[5]

$$-\tilde{u}(\mathbf{k},r)=\sum_{n=1}^{\infty}\sum_{m=0}^{[n/2]}{}_nC_{2m}\,w^{2m}u^{n-2m}(-1)^n(2n\Pi)^{n-1}\ , \tag{4.12}$$

$$-\tilde{v}(\mathbf{k},r)=\sum_{n=1}^{\infty}(-v)^n(n\Pi)^{n-1}\ , \tag{4.13}$$

in which the elementary bubble propagator is defined, as usual,[4,5] by

$$\Pi(\mathbf{k},r)\equiv(2\pi)^{-d}\int d^dp\,g(\mathbf{p})g(\mathbf{p}+\mathbf{k})\ . \tag{4.14}$$

At $r=0$ this behaves as Π_0k^{d-4} as $\mathbf{k}\rightarrow 0$. The series in (4.12) and (4.13) are readily summed and yield

$$\tilde{u}(\mathbf{p})=\frac{u+2n\Pi(u^2-w^2)}{1+4n\Pi u+(2n\Pi)^2(u^2-w^2)}\approx\frac{1}{2n\Pi(\mathbf{p})}\ , \tag{4.15}$$

$$\tilde{v}(\mathbf{p})=\frac{v}{1+nv\Pi(\mathbf{p})}\approx\frac{1}{n\Pi(\mathbf{p})}\ , \tag{4.16}$$

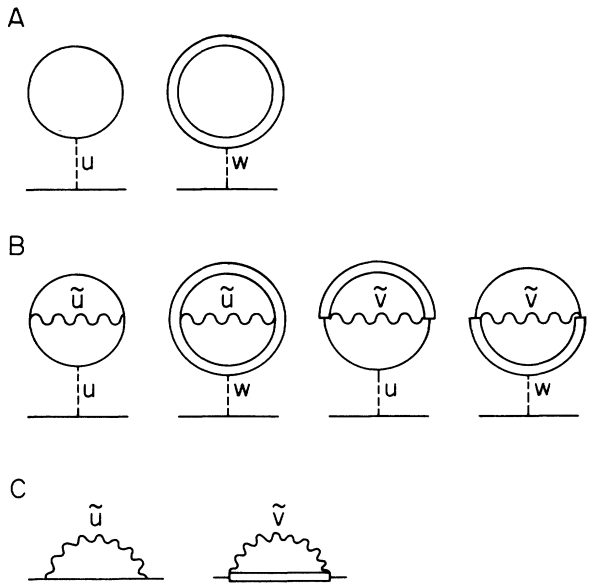

FIG. 5. Self-energy diagrams to $O(1/n)$. Single and double lines represent **a** and **b** propagators, respectively.

as $\mathbf{p}\to 0$ (with $r=0$). Furthermore, diagrams A and B in Fig. 5 do not contribute to $G^{-1}(\mathbf{k},0)$; the term of order $1/n$ comes only from diagram C which yields

$$\Sigma(\mathbf{k},0)-\Sigma(0,0)=\frac{1}{(2\pi)^d}\int d^dp\frac{1}{(\mathbf{k}+\mathbf{p})^2}[4\tilde{u}(\mathbf{p})+\tilde{v}(\mathbf{p})]\ . \tag{4.17}$$

Now η is $O(1/n)$, and so can be obtained from the coefficient of the $k^2\ln k$ term in this integral; that arises from the small-$\mathbf{p}$ region. Using (4.15) and (4.16) then gives the relevant contribution as

$$\Sigma(\mathbf{k},0)-\Sigma(0,0)\sim\frac{3}{n}\frac{1}{(2\pi)^d}\int d^dp\frac{1}{\Pi(\mathbf{p})}\left[\frac{1}{(\mathbf{p}+\mathbf{k})^2}-\frac{1}{\mathbf{p}^2}\right]\ . \tag{4.18}$$

However, except for a factor $\frac{3}{2}$ this has precisely the same form as the corresponding expression for the standard O(n) system.[5] (Indeed, one reproduces the O(n) expression by putting $v=0$ and replacing $2n$ by n.) Thus, using the known O(n) calculation one directly obtains the final result (4.3).

B. Evaluation of γ

To calculate γ, one may similarly study the r dependence of $G(\mathbf{k}=\mathbf{0},r)\equiv\chi^{-1}(r)$ via the relation $\Delta\Sigma\equiv\Sigma(\mathbf{0},r)-\Sigma(\mathbf{0},0)\sim r^{1/\gamma}$ as $r\to 0$. The leading, $O(n^0)$, contribution to $\Delta\Sigma$ comes from diagram A in Fig. 5, which yields $\Delta\Sigma\sim r^{(d-2)/2}$. This simply represents the spherical-model result $\gamma=2/(d-2)$. If one writes $1/\gamma=(d-2)/2-\Delta\Gamma$ with $\Delta\Gamma\sim O(1/n)$, one has

$$\Delta\Sigma\sim r^{(d-2)/2}(1-\Delta\Gamma\ln r+\cdots)\ .$$

Thus, the correction, $\Delta\Gamma$, can be obtained from the $r^{(d-2)/2}\ln r$ term in $\Delta\Sigma$. Diagram C has no such term, while diagram B gives

$$\Sigma_B(\mathbf{k}=\mathbf{0},r)=-2n(u+w)\frac{1}{(2\pi)^d}\times\int d^dq\frac{1}{(r+\mathbf{q}^2)^2}[\Sigma_c(\mathbf{q},r)-\Sigma_c(\mathbf{0},r)]\ , \tag{4.19}$$

with

$$\Sigma_c(\mathbf{q},r)\sim\frac{3}{n}\frac{1}{(2\pi)^d}\int d^dp\frac{1}{\Pi(\mathbf{p},r)}\frac{1}{r+(\mathbf{p}+\mathbf{q})^2}\ , \tag{4.20}$$

as $\mathbf{q}\to\mathbf{0}$. Once again one finds that the only differences from the standard O(n) calculation[5] of γ are simple factors. Utilizing the earlier work yields (4.2).

C. Evaluation of α

To obtain the specific heat exponent α, one may employ scaling relation $\alpha=(2-\eta_E)\nu$ and compute the exponent η_E which describes the critical point decay of the energy-energy correlation function given by

$$C_E(\mathbf{k})=\sum_{\lambda,\mu}\langle[a_\lambda^2(\mathbf{k})+b_\lambda^2(\mathbf{k})][a_\mu^2(-\mathbf{k})+b_\mu^2(-\mathbf{k})]\rangle$$
$$=2(C^{aa}+C^{ab})\ , \tag{4.21}$$

where the decomposition on the second line has the obvious meaning. The leading, $O(n^0)$, diagrams contributing to C^{aa} and C^{ab} are shown in Fig. 6 and lead to

$$C_0^{aa}=2n\Pi(1-\tilde{u}2n\Pi)\sim\frac{u}{u^2-w^2}-\frac{u^2+w^2}{(u^2+w^2)^2}\frac{1}{2\Pi n}\ , \tag{4.22}$$

$$C_0^{ab}=-(2n\Pi)^2\tilde{w}\sim-\frac{w}{u^2-w^2}+\frac{2uw}{(u^2-w^2)^2}\frac{1}{2\Pi n}\ , \tag{4.23}$$

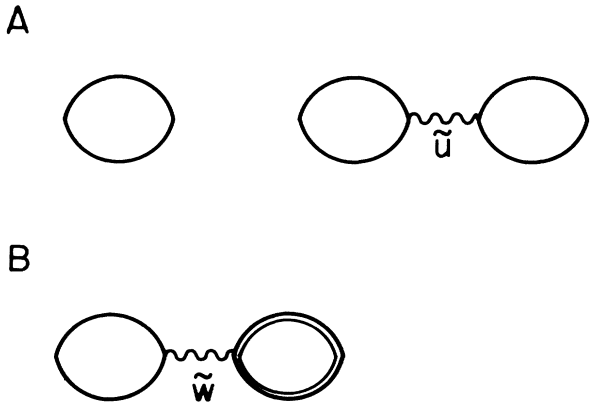

FIG. 6. Leading diagrams appearing in the energy-energy correlation function; A contributes to C^{aa}, and B to C^{ab}.

where the new dressed interaction is given by

$$-\tilde{w}(\mathbf{p})=\sum_{m=1}^{\infty}\sum_{l=0}^{[(m-1)/2]}{}_mC_{2l+1}w^{2l+1}u^{m-(2l+1)}\times(-1)^m(2n\Pi)^{m-1}$$
$$=-w/[(1+2n\Pi u)^2-(2n\Pi w)^2]\ . \quad (4.24)$$

On putting $r=0$ and collecting terms, the $O(n^0)$ result is

$$C_E(\mathbf{k})\approx-\frac{1}{(u+w)^2}\frac{1}{2n\Pi_0}k^{4-d}\ , \quad (4.25)$$

as $\mathbf{k}\to 0$. This merely confirms the spherical-model value $\eta_E=6-d$.

The diagrams for $O(1/n)$ may be constructed from the $O(1/n)$ bubble diagrams Π_1^{aa}, Π_1^{ab}, Π_1^{ba}, Π_1^{bb} shown in Fig. 7, which have (aa), (ab), (ba), (bb) terminals, respectively, by hooking the $O(n^0)$ "arm" diagrams A^{aa}, A^{ab}, A^{ba}, A^{bb} shown in Fig. 8 to both ends of each Π_1. By symmetry one has $\Pi_1^{aa}=\Pi_1^{bb}$, $\Pi_1^{ab}=\Pi_1^{ba}$, and $A^{aa}=A^{bb}$, $A^{ab}=A^{ba}$. In terms of these auxiliary kernels, the $O(1/n)$ part of C^{aa} and C^{ab} can be written as

$$C_1^{aa}=[(A^{aa})^2+(A^{ab})^2]\Pi_1^{aa}+2A^{aa}A^{ab}\Pi_1^{ab}\ , \quad (4.26)$$

$$C_1^{ab}=2A^{aa}A^{ab}\Pi_1^{aa}+[(A^{aa})^2+(A^{ab})^2]\Pi_1^{ab}\ . \quad (4.27)$$

The correction to η_E follows from the coefficient of the $k^{4-d}\ln k$ term. The relevant parts of the bubble diagrams are found to be

$$\frac{\Pi_1^{aa},\Pi_1^{ab}}{8\Pi_0 S_d k^{d-4}\ln k}=\left[\frac{12}{d}+5d-16\right],\quad (d-2)\ . \quad (4.28)$$

The "arm" diagrams give

$$A^{aa}=1-\tilde{u}2n\Pi\sim\frac{u}{u^2-w^2}\frac{1}{2n\Pi}\ , \quad (4.29)$$

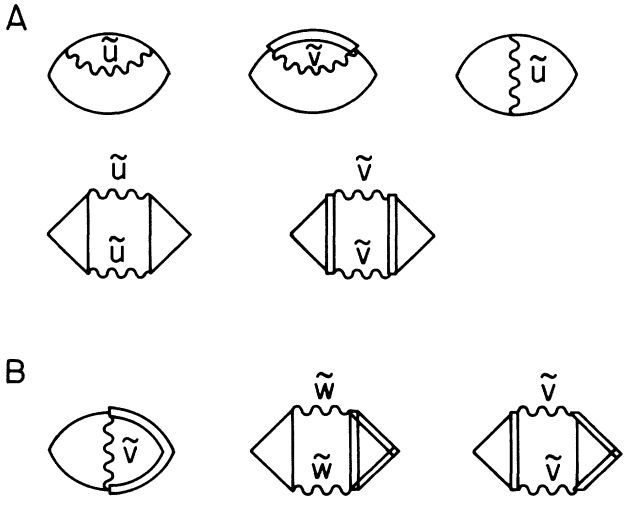

FIG. 7. Bubble diagrams for order $1/n$: A with two a terminals, Π_1^{aa}; B with one a and one b terminal, Π_1^{ab}.

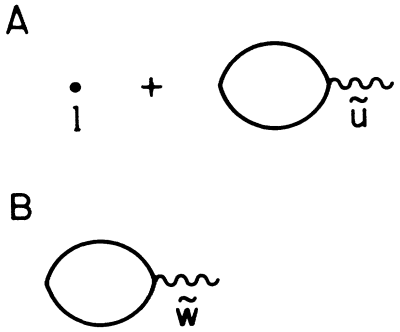

FIG. 8. "Arm" diagrams of order n^0: A, A^{aa} and B, A^{ab}.

$$A^{ab}=-\tilde{w}2n\Pi\sim-\frac{w}{u^2-w^2}\frac{1}{2n\Pi}\ , \quad (4.30)$$

while the dressed interaction $\tilde{w}(\mathbf{p})$ behaves as

$$\tilde{w}(\mathbf{p})\sim\frac{2(2u-v)}{v(4u-v)}\frac{1}{4n^2\Pi_0^2}p^{2(d-4)}\ \text{as}\ \mathbf{p}\to\mathbf{0}\ . \quad (4.31)$$

Evidently, the contribution of $\tilde{w}$ is nonuniversal, depending on u and v, even when $\mathbf{p}\to\mathbf{0}$, in contrast to $\tilde{u}$ and $\tilde{v}$; however, the $\mathbf{p}$ dependence is different from that of $\tilde{u}$ and $\tilde{v}$ and the associated diagram does not contribute to the $k^{d-4}\ln k$ term. By combining (4.21) and (4.26)–(4.30), one thus obtains the full $O(1/n)$ correction for η_E and confirms the results (4.1).

V. CHIRALITY

As explained in the Introduction, in a helical or triangular XY antiferromagnet with $n=2$, the chirality, κ, is an Ising-like scalar variable which, physically, represents the sense of the helix or of the 120° structure.[9] In terms of the $\mathbf{a}$ and $\mathbf{b}$ fields entering the basic GLW Hamiltonian (1.2), the chirality is just the vector product $\mathbf{a}\times\mathbf{b}$, or $\kappa\equiv a_xb_y-a_yb_x$. Under O(2) spin and phase rotations, κ is invariant for proper rotations but changes the sign for *improper* rotations. For n-component spins with $n\geq 3$, there is no longer an Ising-like chirality variable. However, as mentioned in the Introduction, chirality can be extended to an $n\times n$ second-rank antisymmetric tensor variable, $\kappa_{\lambda\mu}=a_\lambda b_\mu-a_\mu b_\lambda$ $(1\leq\lambda,\mu\leq n)$, which has $n(n-1)/2$ independent components. Appendix C expresses $\kappa_{\lambda\mu}$ in terms of the actual spin variables on the lattice. Under O(n) spin rotations, these transform among themselves, whereas under O(2) phase transformation, each component is invariant under proper rotations but changes sign under improper rotations.

One may introduce a conjugate *chiral field*, h_κ, which couples to a component of the chirality via a term $-h_\kappa\kappa_{\lambda\mu}$ in the Hamiltonian. Application of h_κ reduces the original symmetry of the Hamiltonian. Physically speaking, the helical spin structure is then confined to the (λ,μ) plane and one out of two senses of the helix is selected; the degeneracy of the ordered-state manifold is thereby reduced to that of the standard XY model. In

other words, the symmetry of the Hamiltonian is reduced to $SO(2)\times O(n-2)$ spin and SO(2) phase rotations. Thus, under a finite chiral field, the system should crossover from the fully-symmetric chiral behavior to XY criticality.

Naturally, the chiral-field crossover is controlled by a corresponding exponent, ϕ_κ, associated with the original chiral fixed point. The calculation of this chiral crossover exponent, both in the ε and $1/n$ expansions, is sketched in this section. Chirality appears as a new type of relevant operator. At the chiral fixed point, the crossover exponent is found to be

$$\begin{aligned}\phi_\kappa &= 1+\tfrac{1}{4}B_n[n^3+4n^2+56n-96 \\ &\quad +(n^2-24)R_n^{1/2}]\varepsilon+O(\varepsilon^2) \\ &\approx 1+\tfrac{1}{2}(1-8n^{-1})\varepsilon \quad (n\gg 1)\ , \end{aligned} \tag{5.1}$$

while the corresponding result in the $1/n$ expansion is

$$\phi_\kappa=\frac{2}{d-2}\left[1-8\frac{S_d}{n}\right]+O(1/n^2)\ . \tag{5.2}$$

These two expressions coincide for large n as $\varepsilon\to 0$. Comparison with the corresponding expressions (3.9) for γ, shows that the chiral crossover exponent exceeds γ. This is surprising since in previous cases such crossover exponents have satisfied $\phi<\gamma$. Note, however, that the gap exponent $\Delta=\gamma+\beta$, which is really the crossover exponent for the magnetic field, h, does exceed ϕ_κ. As usual, one may write a scaling formula for the singular part of the free energy,

$$f_s\approx t^{2-\alpha}F(h/t^{\Delta},h_\kappa/t^{\phi_\kappa})\ . \tag{5.3}$$

If the total chirality, $\bar{\kappa}=-(\partial f/\partial h_\kappa)_{h_\kappa=0}$, and the chiral susceptibility,

$$\chi_\kappa=\int d\mathbf{r}\langle\kappa_{\lambda\mu}(\mathbf{0})\kappa_{\lambda\mu}(\mathbf{r})\rangle=-(\partial^2 f/\partial h_\kappa^2)_{h_\kappa=0}\ , \tag{5.4}$$

are characterized by critical exponents β_κ and γ_κ, scaling gives

$$\beta_\kappa=2-\alpha-\phi_\kappa,\quad \gamma_\kappa=2\phi_\kappa-(2-\alpha)\ , \tag{5.5}$$

and the chirality exponents satisfy the Essam-Fisher relation $\alpha+2\beta_\kappa+\gamma_\kappa=2$.

At the sinusoidal fixed point, which is stable for $n_{\rm II}(d)>n>n_{\rm III}(d)$ the analog of ϕ_κ is obtained from (5.1) merely by changing the sign of the radical. Now the exponent proves to be *smaller* than the corresponding susceptibility exponent γ. Note, however, that the physical meaning of chirality operator in sinusoidal systems is quite different than in helical systems; indeed, in the sinusoidal case, $\kappa_{\lambda\mu}$ vanishes identically even in the ordered state because the spin ordering is collinear, i.e., $\mathbf{a}\|\mathbf{b}$.

At the $2n$-component Heisenberg fixed point, which is stable for $n<n_{\rm III}(d)\approx 2-\varepsilon$, ϕ_κ reduces to the ordinary anisotropy-crossover exponent,[6]

$$\phi=1+\varepsilon/2(n+4)+O(\varepsilon^2)\ ,$$

which is smaller than the corresponding γ.

The calculations for ϕ_κ proceed as follows. The chirality term, $-h_\kappa(a_1b_2-a_2b_1)$, is added to the Hamiltonian (1.2). To derive the modified recursion relations to $O(\varepsilon)$, it is convenient to transform to new field variables which diagonalize the quadratic part which becomes

$$\begin{aligned}\mathcal{H}_2=\tfrac{1}{2}\Big[&(\nabla\boldsymbol{\alpha})^2+(\nabla\boldsymbol{\beta})^2+(r_0+\tfrac{1}{2}h_\kappa)(\alpha_1^2+\alpha_2^2) \\ &+(r_0-\tfrac{1}{2}h_\kappa)(\beta_1^2+\beta_2^2)+r_0\sum_{\lambda=3}^{n}(\alpha_\lambda^2+\beta_\lambda^2)\Big]\ . \end{aligned} \tag{5.6}$$

Around a fixed point, at which h_κ vanishes, the appropriate renormalization-group eigenexponent is then found to be

$$y_\kappa=2-(4u^*-3v^*)K+O(\varepsilon^2)\ . \tag{5.7}$$

From this, the chirality is seen to be relevant; the crossover exponent is given by $\phi_\kappa=y_\kappa\nu$. Explicit substitution of the previous results for u^*, v^*, and ν yield the values quoted above.

In order to calculate ϕ_κ to $O(1/n)$, the chirality-chirality correlation function

$$C_\kappa(\mathbf{k})=\langle\kappa_{\lambda\mu}(\mathbf{k})\kappa_{\lambda\mu}(-\mathbf{k})\rangle\quad(\lambda\neq\mu)\ , \tag{5.8}$$

is utilized. At $T=T_c$ ($r=0$), this should vary as $k^{\psi\kappa}$ for small $\mathbf{k}$ where $\phi_\kappa=(2-\alpha-\psi_\kappa\nu)/2$. On substituting for $\kappa_{\lambda\mu}$ we get $C_\kappa=2(C^+-C^-)$ where

$$C^+\equiv\langle a_\lambda b_\mu a_\lambda b_\mu\rangle,\quad C^-\equiv\langle a_\lambda b_\mu b_\lambda a_\mu\rangle\ , \tag{5.9}$$

where the spin-component indices, λ and μ ($\lambda\neq\mu$), are held fixed. The leading diagram contributing to C^+ is

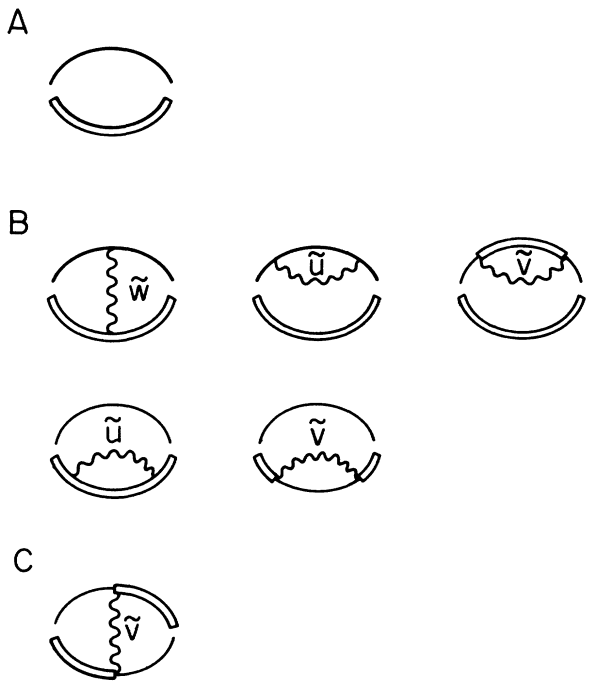

FIG. 9. Diagrams contributing to the correlation function C^+, A at $O(1)$, B at $O(1/n)$, and C one contributing to C^- at $O(1/n)$.

shown in Fig. 9(a) which gives $C_0^+ \approx \Pi_0 k^{d-4}$ as $\mathbf{k} \to \mathbf{0}$. There is no O(1) diagram contributing to C^-, and so one has $\psi_\kappa = d-4$ in leading order. The $O(1/n)$ corrections follow from the coefficient of the $k^{d-4}\ln k$ terms in the diagrams, contributing to C^+ and C^-, shown in Fig. 9(b) and Fig. 9(c), respectively. Actually, the diagram containing $\bar{w}$, does not contribute to ψ_κ because it has no $k^{d-4}\ln k$ singularity. Altogether, one finds

$$\psi_\kappa = d-4+16(3d^{-1}-1)S_d/n + O(n^{-2}) , \tag{5.10}$$

from which the result (5.2) follows.

VI. OTHER CROSSOVER EXPONENTS

In the O(n) Heisenberg model, there is only *one* crossover exponent at quadratic order in the spins, namely, the standard anisotropy-crossover exponent.[16] However, in the present chiral model, as a reflection of the richer underlying symmetry, one should anticipate more than one crossover exponent even at the quadratic level. To study the point, we consider now the most general perturbation which is quadratic in the **a** and **b** fields and search for all eigenoperators and their associated crossover exponents. There are, in total, $2n^2+n-1$ independent quadratic perturbations apart from the energy-density operator, $\mathbf{a}^2+\mathbf{b}^2$. The renormalization-group analysis yields four distinct exponents ϕ_1, ϕ_2, ϕ_3, and ϕ_4. To lowest order in ε, they are given by

$$\phi_i = 1+(2nu^*+C_i v^*)K + O(\varepsilon^2) , \tag{6.1}$$

with

$$C_1=(4-n)/2, \quad C_2=(2-n)/2 ,$$

$$C_3=-n/2, \quad C_4=-(n-1) , \tag{6.2}$$

where u^* and v^* are the fixed-point values previously determined in Sec. III. The associated scaling operators E_i and their degeneracies are listed in Table I. The chirality and its exponent correspond to E_1 and ϕ_1. All eigenoperators belonging to a given ϕ_i are mixed under the symmetry operations of the Hamiltonian; in other words, there is no accidental degeneracy left for any eigenvalue. Thus the existence of the four different crossover exponents should be a general attribute of the model not limited to the ε expansion. Explicit expressions for E_2, E_3, and E_4 in terms of spin variables can be found as in Appendix C. Roughly speaking, E_3 represents the usual anisotropy perturbations, E_2 represents wave-vector–dependent anisotropies, and E_4 represents wave-vector–dependent energy perturbations.

At the *chiral* fixed point, in particular, the inequality

$$\phi_1 > \gamma > \phi_2 > \phi_3 > \phi_4 \tag{6.3}$$

holds. Although the chiral exponent $\phi_\kappa \equiv \phi_1$ exceeds γ, as has been noted, the other three exponents are smaller.

The exponents ϕ_i have also been calculated by the $1/n$ expansions: the results are included in Table I. The same inequality (6.3) is satisfied. In the limit $n \to \infty$, ϕ_1, γ, ϕ_2, and ϕ_3 approach $2/(d-2)$, while ϕ_4 tends to unity. Table I also includes the explicit ε-expansion expressions for ϕ_i at the chiral fixed point. All the ε and $1/n$ expansion results are consistent in the limit $\varepsilon \to 0$ and $n \to \infty$.

TABLE I. Quadratic crossover exponents ϕ_i ($1 \le i \le 4$), the associated scaling operators, $\mathbf{E}_i$, and their degeneracies, D_i. In the first column the upper formula is the ε-expansion result for ϕ_i [see Eqs. (6.1) and (6.2)] evaluated at the chiral fixed point, while the lower formula is the $(1/n)$-expansion result. The functions B_n and R_n are defined by Eqs. (3.4), and $C_n^{(1)} \sim C_n^{(4)}$ are defined by $C_n^{(1)} \equiv n^3+4n^2+56n-96$, $C_n^{(2)} \equiv n^3+52n-48$, $C_n^{(3)} \equiv n^2-4n+48$, and $C_n^{(4)} \equiv n^3+2n^2-76n+48$.

i	ϕ_i	$\mathbf{E}_i$	D_i
1	$1+\frac{1}{4}B_n[C_n^{(1)}+(n^2-24)R_n^{1/2}]$ $(d/2-1)^{-1}(1-8S_d/n)$	$a_\lambda b_\mu - a_\mu b_\lambda$ $(\lambda \neq \mu)$	$\frac{n(n-1)}{2}$
2	$1+\frac{1}{4}B_n[C_n^{(2)}+(n^2-12)R_n^{1/2}]$ $(d/2-1)^{-1}(1-10S_d/n)$	$a_\lambda b_\mu + a_\mu b_\lambda$ $(\lambda \neq \mu)$ $a_\lambda a_\mu - b_\lambda b_\mu$ $(\lambda \neq \mu)$ $\Sigma a_\lambda (a_\lambda^2 - b_\lambda^2)$ $(\Sigma a_\lambda = 0)$ $\Sigma a_\lambda a_\lambda b_\lambda$ $(\Sigma a_\lambda = 0)$	$(n+2)(n-1)$
3	$1+\frac{1}{4}nB_n(C_n^3+nR_n^{1/2}$ $(d/2-1)^{-1}(1-12S_d/n)$	$a_\lambda a_\mu + b_\lambda b_\mu$ $(\lambda \neq \mu)$ $\Sigma a_\lambda (a_\lambda^2 + b_\lambda^2)$ $(\Sigma \alpha_\lambda = 0)$	$\frac{(n+2)(n-1)}{2}$
4	$1-\frac{1}{4}B_n[C_n^{(4)}-(n^2+6n-12)R_n^{12}]$ $1-4S_d/n$	$\mathbf{a}^2-\mathbf{b}^2$ $\mathbf{a}\cdot\mathbf{b}$	2

At the *sinusoidal* fixed point, the relative magnitude of the exponents is

$$\gamma > \phi_4 > \phi_3 > \phi_2 > \phi_1 , \tag{6.4}$$

all four crossover exponents being smaller than γ. The explicit expressions to $O(\varepsilon)$ follow by substituting (3.5) and (3.6) into (6.1) and (6.2).

At the $2n$-component Heisenberg fixed point, one has $v^*=0$ and all four crossover exponents coalesce to a common value, as evident from (6.1). One then has $\gamma > \phi \equiv \phi_i$ (all i).

VII. SUMMARY AND DISCUSSION

The critical properties of the field-theoretic chiral model (1.2) have been studied within renormalization-group theory. This model represents, for positive v, triangular antiferromagnets, helical magnets, and the superfluid A phase of helium 3. By ε expansion, a new chiral fixed point with $v>0$ has been found which is stable for

$$n > n_I(d) \simeq 21.8 - 23.4\varepsilon + O(\varepsilon^2) .$$

The associated susceptibility and the correlation-length exponents γ and ν are smaller than the corresponding O(n) exponents. Likewise, the $1/n$ expansion for (1.2) with $v>0$ yields a continuous transition for $2<d<4$ characterized by exponents γ and ν smaller than the O(n) exponents, and consistent with the ε-expansion results. The nature of chiral ordering was also studied. Chirality represents a new relevant operator; the associated crossover exponent ϕ_κ exceeds γ. Three other crossover exponents are found for perturbations quadratic in the spin variables; these turn out to be smaller than γ.

Concomitantly, the properties of other fixed points were also determined: one represents sinusoidally ordering systems, the other is simply the standard Heisenberg fixed point.

The most interesting question still to be addressed is whether the chiral fixed point remains stable at physically relevant points, namely for $d=3$ with $n=2$ and 3. Although linear extrapolation of the stability boundaries for the chiral fixed point suggests that this might be so, the answer is not conclusive. If the chiral fixed point were not stable, the system would probably undergo a first-order transition. Hopefully, the calculation of higher-order terms combined with fuller analysis will yield a more definitive answer.

It is instructive to compare the present renormalization-group theory with the results of Monte Carlo simulations and experiments. Recent Monte Carlo simulations for $d=3$ XY ($n=2$) (Ref. 9), and Heisenberg ($n=3$) (Ref. 8) antiferromagnets on the stacked-triangular lattice exhibit a single continuous transition, the associated exponents $\alpha \simeq 0.40$, $\beta \simeq 0.25$, $\gamma \simeq 1.1$, and $\nu \simeq 0.53$ for $n=2$, and $\alpha \simeq 0.34$, $\beta \simeq 0.28$, $\gamma \simeq 1.1$, and $\nu \simeq 0.55$ for $n=3$, respectively.[17] Evidently, the estimated values of γ and ν are considerably smaller than the corresponding O(n) values, namely, $\gamma \simeq 1.32$ and $\nu \simeq 0.67$ for $n=2$, and $\gamma = 1.38$ and $\nu \simeq 0.70$ for $n=3$.[18] These Monte Carlo data, particularly the observation of a continuous transition and the small γ and ν values, do indeed suggest that the chiral fixed point remains stable for $n=2$ and 3 down to $d=3$. More recently[9b] the chirality exponents themselves have been estimated for the XY case ($n=2$) with the results $\beta_\kappa \simeq 0.40$, $\gamma_\kappa \simeq 0.80$, and $\phi_\kappa = \beta_\kappa + \gamma_\kappa \simeq 1.20$. These exponents satisfy the scaling relation $\alpha + 2\beta_\kappa + \gamma_\kappa = 2$ as anticipated. Furthermore, the chiral crossover exponent is larger than γ as our RG theory indicates. Thus, all Monte Carlo results obtained so far are consistent with the existence of the stable chiral fixed point in three dimensions.

Experimentally, continuous transitions have been reported for various substances, including triangular antiferromagnets, helical magnets, and helium 3, which are expected to belong to the present universality classes. In particular, recent measurements on VCl_2, VBr_2, $CsMnBr_3$, Ho, and Dy have yielded exponents fairly close to the predicted theoretical values.[17] Further discussion of the experimental aspects of this question has been presented in Ref. 17.

In summary, the overall qualitative agreement found between the renormalization-group theory, the Monte Carlo data, and the experimental results seems to support the view that a series of new chiral universality classes, characterized by the field-theoretic model (1.2), are actually realized in nature.

ACKNOWLEDGMENTS

The author is particularly indebted to Professor Michael E. Fisher for discussions and for reading the manuscript. Part of the present work was done at Cornell University. Thanks are due to the U.S. National Science Foundation for partial support through the Condensed Matter Theory Program (under Grant Nos. DMR-87-01223 and DMR-87-96299), and to the Nishina Memorial Foundation for partial financial support.

APPENDIX A: DERIVATION OF THE GLW HAMILTONIAN

In this appendix, the effective Hamiltonian (1.2) is derived from microscopic spin Hamiltonians like (2.1) or (2.2). Starting with n-component fixed-length spins, $\mathbf{S}_i$, with general isotropic couplings, K_{ij}, one can apply the Hubbard-Stratonovich transformation in the standard way to obtain an equivalent Hamiltonian

$$\mathcal{H} = \tfrac{1}{2} \sum_{\substack{i,j=1 \\ (i\neq j)}}^{N} P_{ij} \boldsymbol{\phi}_i \cdot \boldsymbol{\phi}_j + \sum_i \overline{W}(\, | \boldsymbol{\phi}_i | \,) , \tag{A1}$$

in terms of new unconstrained n-component spins, $\boldsymbol{\phi}_i$.[19] The new interactions, P_{ij}, are given by the matrix relation $[P_{ij}] = [P_0 \delta_{ij} + K_{ij}]^{-1}$, where P_0 is a constant sufficiently large to make $[P_{ij}]^{-1}$ positive definite. The single-spin weighting function is given by

$$\overline{W}(\, | \boldsymbol{\phi}_i | \,) = \tfrac{1}{2} P_{ii} \boldsymbol{\phi}_i^2 - \ln[\mathrm{Tr}_S (e^{-\boldsymbol{\phi}_i \cdot S})] . \tag{A2}$$

If this is expanded out to quartic order and translational invariance of the lattice is invoked, one obtains

$$\mathcal{H}=\sum_{\mathbf{q}}[\bar{r}_0+P(\mathbf{q})]\,|\,\boldsymbol{\phi}(\mathbf{q})\,|^2 + \frac{\bar{u}_0}{V}\sum{}'\boldsymbol{\phi}(\mathbf{q}_1)\cdot\boldsymbol{\phi}(\mathbf{q}_2)\boldsymbol{\phi}(\mathbf{q}_3)\cdot\boldsymbol{\phi}(\mathbf{q}_4)\ , \tag{A3}$$

in which the second sum is restricted, as usual, by $\mathbf{q}_1+\mathbf{q}_2+\mathbf{q}_3+\mathbf{q}_4=\mathbf{K}$, where $\mathbf{K}$ is a reciprocal lattice vector. The parameters are given by

$$\bar{r}_0=\tfrac{1}{2}P_{ii}+\frac{\pi^{1+n/2}}{n+2}\Gamma(\tfrac{1}{2}(n-1))\ , \qquad \bar{u}_0=\frac{\pi^{1+n/2}\Gamma(\tfrac{1}{2}(n-1))}{4(n+4)(n+2)}\ , \tag{A4}$$

while $P(\mathbf{q})$ and $\boldsymbol{\phi}(\mathbf{q})$ are the Fourier transforms of P_{ij} and $\boldsymbol{\phi}_i$.

For concreteness, focus now on the stacked or layered triangular lattice and suppose that $P(\mathbf{q})$ has a *maximum* at $\mathbf{q}=0$ but equivalent *minima* at (dimensionless) wave numbers, $\pm\mathbf{Q}$ with $\mathbf{Q}=(4\pi/3,0,\ldots,0)$ in the lattice layers. The first Brillouin zone for the layers is shown in Fig. 10: note equivalent minimal points differing only by the reciprocal-lattice vectors $\mathbf{K}_1=(2\pi,\ -2\pi/\sqrt{3},\ 0,\ldots,0)$ and $\mathbf{K}_2=(0,\ 4\pi/\sqrt{3},\ 0,\ldots,0)$, just two are independent. The zone can be divided, as shown in the figure, and rearranged into three separate hexagonal subzones centered on the origin, each corresponding to a $\sqrt{3}\times\sqrt{3}$ rotated sublattice. Correspondingly, the field $\boldsymbol{\phi}(\mathbf{q})$ over the original zone can be decomposed uniquely into three fields $\mathbf{A}_\mathbf{q}$, $\mathbf{B}_\mathbf{q}$, and $\mathbf{C}_\mathbf{q}$, where $\mathbf{q}$ is now confined to the new subzone. The original reality condition $\boldsymbol{\phi}^*(\mathbf{q})=\boldsymbol{\phi}(-\mathbf{q})$ yields

$$\mathbf{A}_\mathbf{q}^*=\mathbf{B}_{-\mathbf{q}},\quad \mathbf{B}_\mathbf{q}^*=\mathbf{A}_{-\mathbf{q}},\quad \mathbf{C}_\mathbf{q}^*=\mathbf{C}_{-\mathbf{q}}\ . \tag{A5}$$

Evidently, the two independent "instability" points, associated with the minima of $P(\mathbf{q})$ now occur *at* the *origin* and pertain only to the $\mathbf{A}$ and $\mathbf{B}$ fields. Since the $\mathbf{C}$ modes correspond to a maximum in $P(\mathbf{q})$ they should become rapidly negligible after initial renormalization and, accordingly, will be neglected henceforth. Retaining on the critical modes yields

$$\mathcal{H}=\sum_{\mathbf{q}}[\bar{r}_0+P(\mathbf{q})](\,|\,\mathbf{A}_\mathbf{q}\,|^2+|\,\mathbf{B}_\mathbf{q}\,|^2) + \frac{\bar{u}_0}{V}\sum{}'(2\,\mathbf{A}_{\mathbf{q}_1}\cdot\mathbf{A}_{\mathbf{q}_2}\mathbf{B}_{\mathbf{q}_3}\cdot\mathbf{B}_{\mathbf{q}_4} +4\,\mathbf{A}_{\mathbf{q}_1}\cdot\mathbf{B}_{\mathbf{q}_2}\mathbf{A}_{\mathbf{q}_3}\cdot\mathbf{B}_{\mathbf{q}_4})\ , \tag{A6}$$

the second sum being restricted as before. Note that quartic terms of the form A^4, A^3B, AB^3, and B^4 do not appear because of the wave-number–conservation conditions. Renormalization and removal of the C modes will, of course, change the coefficient $\bar{r}_0$ and the transform $P(\mathbf{q})$ somewhat but, as usual, an expansion and transverse spatial rescaling should serve to justify the expansion

$$P(\mathbf{q})=c_0+c_1\mathbf{q}^2+O(\mathbf{q}^4)\ . \tag{A7}$$

Finally, we introduce two *real* n-component fields by

$$\mathbf{a}=\tfrac{1}{2}(\mathbf{A}+\mathbf{B}),\quad \mathbf{b}=-\tfrac{1}{2}i(\mathbf{A}-\mathbf{B}) \tag{A8}$$

so that $\mathbf{a}_\mathbf{q}^*=\mathbf{a}_{-\mathbf{q}}$, $\mathbf{b}_\mathbf{q}^*=\mathbf{b}_{-\mathbf{q}}$. It follows that $\mathbf{a}_\mathbf{q}$ and $\mathbf{b}_\mathbf{q}$ describe pure cosine and sine modes, i.e., $\cos[(\mathbf{Q}+\mathbf{q})\cdot\mathbf{r}]$ and $\sin[(\mathbf{Q}+\mathbf{q})\cdot r]$, respectively. Rewriting (A6) in terms of the $\mathbf{a}$ and $\mathbf{b}$ fields and Fourier inversion leads to

$$\mathcal{H}=\int d^dx\{2c_1(\,|\,\nabla\mathbf{a}\,|^2+|\,\nabla\mathbf{b}\,|^2)+2(\bar{r}_0+c_0)(\mathbf{a}^2+\mathbf{b}^2) +6\bar{u}_0(\mathbf{a}^2+\mathbf{b}^2)^2+8\bar{u}_0[(\mathbf{a}\cdot\mathbf{b})^2-\mathbf{a}^2\mathbf{b}^2]\}\ . \tag{A9}$$

By simple spin rescaling then yields (1.2) with, ignoring initial renormalization effects,

$$r_0=(\bar{r}_0+c_0)/c_1,\quad u=3\bar{u}_0/4c_1^2,\quad v=\bar{u}_0/c_1^2\ . \tag{A10}$$

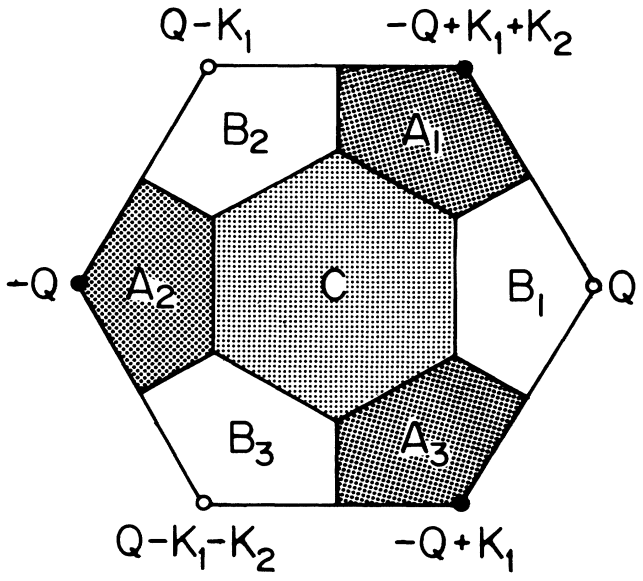

FIG. 10. Two-dimensional intersection of the first Brillouin zone of the d-dimensional stacked-triangular lattice, cut by the plane $q_3=\cdots=q_d=0$. The first Brillouin zone is divided into three similar subdomains (A_1, A_2, A_3), (B_1, B_2, B_3), and C.

APPENDIX B: CALCULATION OF η

In this appendix, η is calculated to $O(\varepsilon^2)$ at the chiral fixed point. The notation follows that in Secs. III–V. As explained in Sec. IV, η can be obtained from the coefficient of the $k^2\ln k$ term of the self-energy difference at $T=T_c$, namely,

$$\Sigma(\mathbf{k},r=0)-\Sigma(\mathbf{k}=0,r=0)\ .$$

The diagrams needed to $O(\varepsilon^2)$ are shown in Fig. 11 where $w=u-\frac{1}{2}v$. From these one gets

$$\eta=[16(n+1)u_0-8(n-1)u_0v_0 +3(n-1)v_0^2]/(16\pi^2)^2\ , \tag{B1}$$

where u_0 and v_0 are determined so as to eliminate the slow transients,[3] namely contributions from the two irrelevant variables which have exponents of order ε. To this end one may calculate

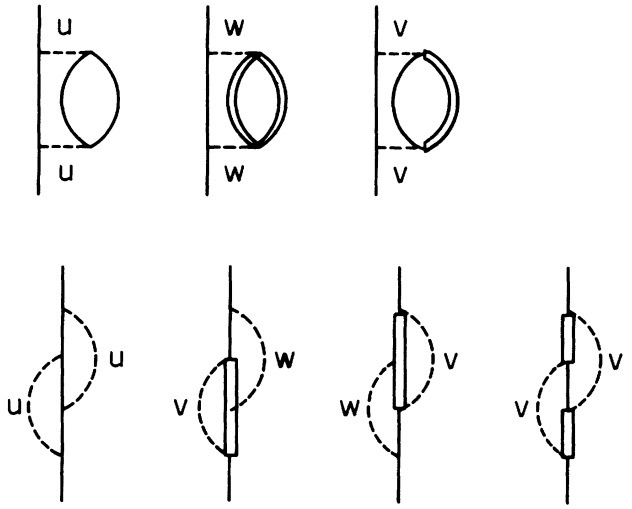

FIG. 11. Diagrams contributing to η to $O(\varepsilon^2)$.

$$\Gamma_4^{aa}(r)\equiv -V\lim_{\mathbf{k}_i\to 0}\langle a_{i\mathbf{k}_1}a_{i\mathbf{k}_2}a_{j\mathbf{k}_3}a_{j\mathbf{k}_4}\rangle_c \Big/ \prod_{i=1}^{4} G(\mathbf{k}_i)\ , \tag{B2}$$

$$\Gamma_4^{ab}\equiv -V\lim_{\mathbf{k}_i\to 0}\langle a_{i\mathbf{k}_1}a_{i\mathbf{k}_2}b_{j\mathbf{k}_3}b_{j\mathbf{k}_4}\rangle_c \Big/ \prod_{i=1}^{4} G(\mathbf{k}_i)\ , \tag{B3}$$

where $\mathbf{k}_1+\cdots+\mathbf{k}_4=0$. From the requirement of no slow transients in Γ_4^{aa} and Γ_4^{ab}, one obtains two sets of solutions for (u_0,v_0): their values agree precisely with the $O(\varepsilon)$ fixed-point values at the chiral and sinusoidal (or antichiral) fixed points, (3.5) and (3.6). By substituting for u_0 and v_0 in (B1) with the *chiral* fixed point values the result (3.10) with (3.4) and (3.11) is found.

APPENDIX C: CHIRALITY TENSOR

In this appendix, we rewrite the total chirality tensor, $\bar{\kappa}_{\lambda\mu}$, in terms of spin operators, $\mathbf{S}_\mu$. After the Fourier transformation, one has

$$\begin{aligned}\bar{\kappa}_{\lambda\mu}&=\int \kappa_{\lambda\mu}(\mathbf{r})d\mathbf{r}=\int (a_\lambda b_\mu - a_\mu b_\lambda)d\mathbf{r}\ ,\\ &=\sum_{\mathbf{q}}[a_\lambda(\mathbf{q})b_\mu(-\mathbf{q})-a_\mu(\mathbf{q})b_\lambda(-\mathbf{q})]\ ,\end{aligned} \tag{C1}$$

where the summation runs over wave vectors $|\mathbf{q}|<|\mathbf{Q}|$, $\mathbf{Q}$ being the wave vector characterizing the helix. On using (A8) to replace the a_λ and b_μ by the A_λ and B_μ and noting that $\mathbf{A}(\mathbf{q})=\mathbf{S}(\mathbf{Q}+\mathbf{q})$ and $\mathbf{B}(\mathbf{q})=\mathbf{S}(-\mathbf{Q}+\mathbf{q})$, we get

$$\begin{aligned}\bar{\kappa}_{\lambda\mu}=\tfrac{1}{2}i\sum_{\mathbf{q}}[&S_\lambda(\mathbf{Q}+\mathbf{q})S_\mu(-\mathbf{Q}-\mathbf{q})\\ &-S_\mu(\mathbf{Q}+\mathbf{q})S_\lambda(-\mathbf{Q}-\mathbf{q})]\ .\end{aligned} \tag{C2}$$

Fourier transforming into real space finally yields

$$\begin{aligned}\bar{\kappa}_{\lambda\mu}&=\sum_{i,j} g_c(\mathbf{r}_{ij})\sin(\mathbf{Q}\cdot\mathbf{r}_{ij})S_\lambda(\mathbf{r}_i)S_\mu(\mathbf{r}_j)\ ,\\ &=\sum_{i>j} g_c(\mathbf{r}_{ij})\sin(\mathbf{Q}\cdot\mathbf{r}_{ij})[S_\lambda(\mathbf{r}_i)S_\mu(\mathbf{r}_j)\\ &\qquad -S_\mu(\mathbf{r}_i)S_\lambda(\mathbf{r}_j)]\ ,\end{aligned} \tag{C3}$$

where $g_c(\mathbf{r})$ is a cut-off function defined by

$$g_c(\mathbf{r})=N^{-1}\sum_{|\mathbf{q}|<Q} e^{i\mathbf{q}\cdot\mathbf{r}}\ , \tag{C4}$$

which becomes small if $|\mathbf{r}|>2\pi/Q$. The expression (C3) essentially constitutes our definition of chirality. In the particular case of triangular antiferromagnets, if one approximates $g_c(\mathbf{r})$ by a step function which vanishes beyond the nearest-neighboring sites, (C3) is exactly proportional to our original definition of chirality, (1.4).

*Permanent address: Department of Physics, College of General Education, Osaka University, Toyonaka-shi, Osaka 560, Japan.

[1]K. G. Wilson, Phys. Rev. B **4**, 3174 (1971); **4**, 3814 (1971).
[2]K. G. Wilson and M. E. Fisher, Phys. Rev. Lett. **28**, 248 (1972).
[3]K. G. Wilson, Phys. Rev. Lett. **28**, 540 (1972).
[4]R. Abe, Prog. Theor. Phys. **48**, 1414 (1972); **49**, 113 (1973).
[5]S. K. Ma, Phys. Rev. A **7**, 2172 (1973).
[6]See, for example, A. Aharony, in *Phase Transition and Critical Phenomena,* edited by C. Domb and M. S. Green (Academic Press, New York, 1976), Vol. VI.
[7]H. Kawamura, J. Appl. Phys. **61**, 3590 (1987).
[8]H. Kawamura, J. Phys. Soc. Jpn. **54**, 3220 (1985); **56**, 474 (1987).
[9](a) H. Kawamura, J. Phys. Soc. Jpn. **55**, 2095 (1986); (b) (unpublished).
[10]H. Kawamura, J. Phys. Soc. Jpn. **55**, 2157 (1986).
[11]T. Garel and P. Pfeuty, J. Phys. C **9**, L245 (1976).
[12]D. R. T. Jones, A. Love, and M. A. Moore, J. Phys. C **9**, 743 (1976).
[13]D. Bailin, A. Love, and M. A. Moore, J. Phys. C **10**, 1159 (1977).
[14]P. Bak and D. Mukamel, Phys. Rev. B **13**, 5086 (1976).
[15]H. Kawamura, Phys. Rev. B (to be published); (unpublished).
[16]M. E. Fisher and P. Pfeuty, Phys. Rev. B **6**, 1889 (1972).
[17]H. Kawamura, J. Appl. Phys. **63**, 3086 (1988).
[18]J. C. Le Guillou and J. Zinn-Justin, Phys. Rev. Lett. **39**, 95 (1977).
[19]M. E. Fisher, in *Critical Phenomena,* Vol. 186 of *Lecture Notes in Physics,* edited by F. J. W. Hahne (Springer-Verlag, Berlin, 1983).